# H Atom and $H_2$ Elimination from Y + $C_2H_2$

**Eric D. Glendening***

*Department of Chemistry, Indiana State University, Terre Haute, Indiana 47809*

*Received: August 28, 2003; In Final Form: August 9, 2004*

Potential energy surfaces are evaluated for H atom and $H_2$ elimination in the gas phase reaction of a Y atom with acetylene, $C_2H_2$. Coupled-cluster calculations are performed with extrapolations to the complete basis set limit and zero point energy, core correlation, and spin−orbit corrections. The resulting surfaces reveal that the lowest energy reaction channel leads to $H_2$ elimination, consistent with the $YC_2 + H_2$ products observed in crossed molecular beam experiments. This reaction proceeds in three steps: (i) $YC_2H_2$ adduct formation, (ii) C−H insertion, and (iii) 1,3-elimination of $H_2$. A higher energy reaction channel leads from the C−H insertion intermediate to the H atom elimination products $YC_2H + H$. Our calculations predict product asymptotes of −7.1 kcal/mol for $YC_2 + H_2$ and 15.0 kcal/mol for $YC_2H + H$, energies that differ considerably from those (−18.5 ± 4.3 and 21.5 ± 2.0 kcal/mol, respectively) determined in the beam experiments. Natural bond orbital methods are used to determine how the metal atom influences the redistribution of electrons during the reaction steps. The open-shell metal atom and its partially occupied valence 4d shell usually promote homolytic cleavage and formation of bonds as the reaction proceeds. Our best estimates of the bond dissociation energies $D_0$(Y−$C_2$), $D_0$(Y−$C_2$H), and $D_0$(H−$YC_2$H) are 147.7, 115.8, and 57.1 kcal/mol, respectively.

## I. Introduction

Crossed molecular beam and fast flow reactor methods have been used to study the fundamental gas phase reactions of neutral metal atoms with simple organic molecules.[1−12] Energetics, rate data, and product distributions are of particular interest in these studies as they provide insight into the mechanisms by which organometallic reactions proceed. Considerable effort has recently focused on reactions of the second row transition metals with small hydrocarbons[1−9] and carbonyl-containing compounds.[10−12] For example, reactions have been reported for Y atoms with $C_2H_2$,[2] $C_2H_4$,[3] $C_2H_6$,[4] *c*-$C_3H_6$,[5] $CH_2O$,[10,11] $CH_3$-CHO,[11] $CH_3COCH_3$,[11] and $CH_2CO$.[12] Reactions for the metal atoms Zr,[1,2,5−8] Nb,[1,2,5,7] and Mo[1,5,9] have also been reported.

We describe here a computational study of one of the simplest metal/hydrocarbon reactions, the reaction of ground state yttrium atom (Y) with acetylene ($C_2H_2$). Davis et al.[2] studied the Y + $C_2H_2$ reaction using crossed molecular beams, and Siegbahn[13,14] calculated several of the key intermediate structures and the metal insertion step. Three reaction channels were examined in the experimental work: (i) $H_2$ elimination yielding products $YC_2$ + $H_2$, (ii) H atom elimination yielding products $YC_2H$ + H, and (iii) nonreactive decay of the collision complexes to reactants Y + $C_2H_2$. $H_2$ elimination was observed at all collision energies studied (6−25 kcal/mol), suggesting an upper bound of 6 kcal/mol for the highest barrier along this reaction pathway. H atom elimination was only observed above collision energies of 21.5 ± 2.0 kcal/mol. A reaction mechanism was proposed, based in part on Siegbahn's calculations, in which the $H_2$ elimination reaction proceeds in four steps. Our objective in this work is to use high level electronic structure methods together with recently developed correlation consistent basis sets for Y to confirm the mechanism and energetics for the Y + $C_2H_2$ reaction. A related computational study of the acetylene (HCCH)−vinylidene ($CCH_2$) rearrangement on Na, Al, and Y atoms is reported elsewhere.[15]

## II. Calculations

Geometry optimizations were performed at the DFT level of theory using the B3LYP functional[16] and polarized double-ζ quality basis sets for all atoms. Dunning's correlation consistent double-ζ basis sets (aug-cc-pVDZ)[17] were employed for H and C, while the Stuttgart 28-electron quasirelativistic effective core potential[18] and Peterson's cc-pVDZ-PP (7s7p5d1f)/[4s4p3d1f] valence basis set[19] were used for Y. Calculations at this level are referred to as B3LYP/aVDZ. The identities (equilibrium, transition state) of all stationary points were determined by frequency calculations, and zero point energy (ZPE) corrections were applied to all energies. Intrinsic reaction coordinate (IRC) calculations of the transition states were performed to identify reaction pathways. B3LYP geometry optimization, frequency, and IRC calculations were performed with Gaussian 98[20] using Gaussian's "tight" convergence threshold to ensure adequate convergence of all geometrical features.

The energies of the B3LYP/aVDZ geometries were evaluated using the restricted coupled-cluster method RCCSD(T) with double-, triple-, and quadruple-ζ basis sets (aug-cc-pV*X*Z for H and C, cc-pV*X*Z-PP for Y[19]). The triple- and quadruple-ζ basis sets for Y are respectively [6s6p4d2f1g] and [7s7p5d3f2g1h] contractions of the (10s10p7d2f1g) and (12s12p9d3f2g1h) primitive sets. The RCCSD(T) energies at the complete basis set limit, *E*(CBS), were estimated by extrapolating the correlation consistent energies, *E*(*X*), using the mixed (exponential + Gaussian) fitting function[21]

$$E(X) = E(\mathrm{CBS}) + Ae^{-(X-1)} + Be^{-(X-1)2} \qquad (1)$$

*X* in this equation represents the cardinal number of the basis set (*X* = 2, 3, and 4 for DZ, TZ, and QZ, respectively) and *E*(CBS), *A*, and *B* are fitting parameters.

* E-mail: glendening@indstate.edu.

10.1021/jp031027i CCC: $27.50 
Published on Web 10/15/2004

**TABLE 1: Energies of the Intermediates, Transition States, and Products of the Y + $C_2H_2$ Reaction.[a,b]**

| | structure | state | B3LYP $S^2$ | B3LYP/aVDZ | RCCSD(T)/aVDZ | RCCSD(T)/aVTZ | RCCSD (T)/aVQZ | CBS[c] | core[d] | best estimate[e] |
|---|---|---|---|---|---|---|---|---|---|---|
| **1b** | $YC_2H_2$ | $^2B_2$ | 0.797 | −24.5 | −25.6 | −25.3 | −25.6 | −25.8 | −0.8 | −25.8 |
| $\mathbf{TS_{add}}$[f] | | $^2A'$ | 0.800 | −19.6 | −20.4 | −19.5 | −19.6 | −19.6 | −0.6 | −19.3 |
| **1a** | $YC_2H_2$ | $^2A_1$ | 0.751 | −48.5 | −44.3 | −44.5 | −45.4 | −45.9 | −1.7 | −46.8 |
| $\mathbf{TS_{ins}}$ | | $^2A'$ | 0.815 | −8.7 | −2.6 | −2.2 | −2.7 | −3.1 | −0.5 | −2.7 |
| **2** | $HYC_2H$ | $^2A'$ | 0.751 | −43.6 | −43.8 | −43.8 | −44.3 | −44.6 | 1.6 | −42.1 |
| $\mathbf{TS_{elim}}$ | | $^2A$ | 0.751 | 0.9 | 0.6 | 1.9 | 1.3 | 0.8 | −0.7 | 1.0 |
| **3** | $H_2{\cdot\cdot}YC_2$ | $^2A_1$ | 0.752 | −4.3 | −7.6 | −6.9 | −7.4 | −7.7 | −0.2 | −7.0 |
| $\mathbf{TS_{\beta H}}$ | | $^2A$ | 0.763 | 9.7 | 8.5 | 11.5 | 11.3 | 11.1 | −0.1 | 11.9 |
| **4** | $H_2YC_2$ | $^2A_1$ | 0.765 | 4.1 | −4.2 | −0.4 | −0.3 | −0.3 | 2.9 | 3.5 |
| $\mathbf{TS_{red}}$ | | $^2A$ | 0.771 | 19.9 | 23.8 | 26.2 | 25.9 | 25.5 | 0.0 | 26.4 |
| | $YC_2 + H_2$ | $^2A_1$, $^1\Sigma_g^+$ | | −5.0 | −7.7 | −7.0 | −7.5 | −7.8 | −0.2 | −7.1 |
| | $YC_2H + H$ | $^1\Sigma^+$, $^2S$ | | 17.9 | 11.2 | 13.3 | 13.3 | 13.3 | 0.8 | 15.0 |

[a] All energies are given in kcal/mol. B3LYP and RCCSD(T) energies include ZPE corrections and are reported relative to the energies of the separated Y + $C_2H_2$ reactants. Deviations of the B3LYP $S^2$ values from a nominal value of 0.75 reflect slight spin contamination in the calculated densities. $S^2$ values for Y atom and $YC_2$ are 0.808 and 0.752, respectively. [b] Basis sets employed are the aug-cc-pV*X*Z sets for H and C and the cc-pV*X*Z-PP sets for Y (*X* = D, T, Q). [c] Estimates of the complete basis set (CBS) limit are obtained by extrapolating the raw RCCSD(T) energies using eq 1. [d] Core-correlation effect is evaluated as the difference of the energies of correlated-core (4s, 4p for Y only, the C 1s electrons remain uncorrelated) and frozen-core calculations. The triple-ζ, core-valence cc-pVTZ-PP basis set is used for Y in these calculations. [e] Best estimate is the sum of the CBS energy, the core-correlation correction, and a calculated spin−orbit correction of 0.9 kcal/mol for the ground $^2D_{3/2}$ state of the isolated Y atom. [f] $\mathbf{TS_{add}}$ optimizations failed to fully converge. See text for discussion.

Core correlation and spin−orbit effects were evaluated for several of the Y-containing structures. Correlation of the Y 4s and 4p electrons was treated at the triple-ζ level using Peterson's cc-pVTZ-PP basis set for Y (aug-cc-pCVTZ for C and H).[19] The cc-pVTZ-PP set includes tight correlating s, p, d, and f shells. Core correlation corrections were evaluated as the difference of frozen-core and core-correlated energies. Correlation of the C 1s electrons was not considered. Spin−orbit (SO) effects were evaluated using the SO operators of Andrae et al.[18] in multireference configuration interaction (MRCI) calculations. The reference wave function was generated from all excitations of the three Y valence electrons within an active space consisting of the 5s and 4d orbitals. The predicted SO splitting for the Y $^2D$ ground state is 545 $cm^{-1}$, in excellent agreement with the experimental splitting[2] of 530 $cm^{-1}$. SO interaction stabilizes the $^2D_{3/2}$ state by 308 $cm^{-1}$ (∼0.9 kcal/mol) relative to the energy of the zero order $^2D$ states. Similar treatment of SO effects in several of the reaction intermediates and transition states was performed. In all cases, the ground electronic state is considerably more stable than any excited state (typically by 5000−6000 $cm^{-1}$), so that SO coupling is weak (usually just a few $cm^{-1}$) and can be neglected. All RCCSD(T) and MRCI/SO calculations were performed with MOLPRO.[22]

Table 1 reports our best estimates for the energies of the intermediates, transition states, and products of the Y + $C_2H_2$ reaction. These estimates are obtained by extrapolating the RCCSD(T) energies (with ZPE corrections) to the CBS limit, then adding a core correlation correction and a SO correction of 0.9 kcal/mol (the stabilization of the ground $^2D_{3/2}$ state of Y). Spin contamination in the unrestricted B3LYP densities, reflected in the slight deviations of the $S^2$ value from the nominal doublet value of 0.75, was judged to be reasonably small. The calculated reaction pathways are displayed in Figure 1 and will be discussed in detail in the following section. Figures 2−4 show the B3LYP/aVDZ optimized geometries for the $YC_2H$ and $YC_2$ products, reaction intermediates, and transition states.

The natural bond orbital (NBO) method[23] was used to identify the best Lewis representations of the equilibrium geometries and to determine how the electrons of the reactants undergo redistribution as products form. Redistribution was usually determined by examining the character of the natural localized molecular orbitals (NLMOs) along the reaction pathway. As discussed elsewhere,[15] only one or two NLMOs typically undergo a change of character during a reaction step. For example, as one proceeds along a pathway, a lone pair type NLMO of the reactant may increasingly delocalize into an acceptor orbital of an adjacent atom, strengthening the covalent interaction between the two atoms and eventually leading to the formation of a bond in the product. This "chemically active" NLMO can be readily identified in the transition state due to the strong mixing of the lone pair and acceptor orbitals. Natural population analysis (NPA) was used to identify the distribution of charge and spin density in the equilibrium and transition states. NPA results are given in Table 2 and will be referred to throughout our discussion.

## III. Results

**A. H Atom and $H_2$ Elimination Products.** Davis et al.[2] have studied reactive collisions of Y atoms with $C_2H_2$ using crossed molecular beams. Collisions yield either H atom elimination products ($YC_2H$ + H) or $H_2$ elimination products ($YC_2$ + $H_2$), with the latter corresponding to the lower energy reaction channel. $YC_2H$ + H products were only observed at collision energies above 21.5 ± 2.0 kcal/mol, whereas $YC_2$ + $H_2$ products were observed at all energies between 6 and 25 kcal/mol. Our calculations predict product asymptotes of 15.0 kcal/mol for $YC_2H$ + H and −7.1 kcal/mol for $YC_2$ + $H_2$. Unless indicated otherwise, all energies reported here are relative to that of the separated Y + $C_2H_2$ reactants.

H atom elimination yields yttrium acetylide ($YC_2H$). $YC_2H$ is a linear molecule in its ground $^1\Sigma^+$ state (Figure 2) with a Y−C distance of 2.256 Å. A nonbonding electron pair occupies a Y orbital of principally 5s character, and a Y−C bond forms from the overlap of the Y $4d_{z^2}$ with a C sp hybrid. The bond is predominantly ionic and is strongly polarized (by 88%) toward the C atom, as evidenced by the large partial charge (+0.75) on Y. The $\pi$-bonding interactions of acetylide with the Y $4d_{xz}$ and $4d_{yz}$ orbitals are weak, as noted previously by Siegbahn.[14] The pair of $\pi \rightarrow$ 4d interactions back transfer only 0.05 e to Y. Our best estimate of the Y−C dissociation energy, $D_0$(Y−$C_2H$), is 115.8 kcal/mol, in excellent accord with the Siegbahn's PCI-80 estimate of 116.5 kcal/mol[14] and in fair agreement with the experimental value of 110.2 ± 2.0 kcal/mol.[2] As shown in Figure 1, our calculations suggest that H atom elimination proceeds via a three step mechanism. These steps include (i)

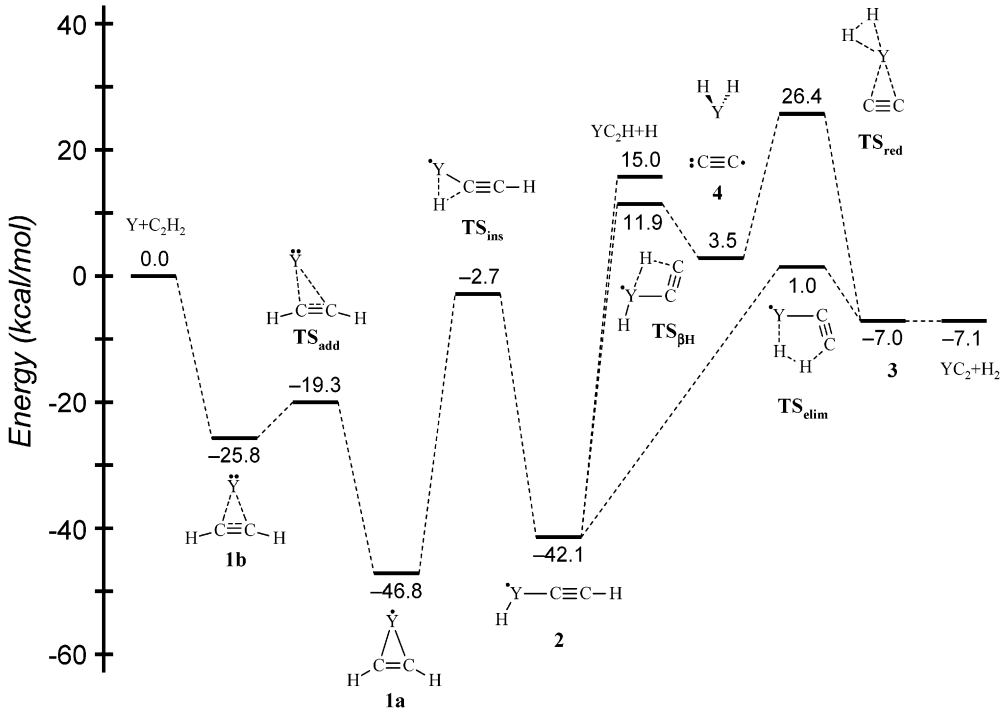


**Figure 1.** Calculated pathways for the elimination of H atom and $H_2$ from the Y + $C_2H_2$ reaction.

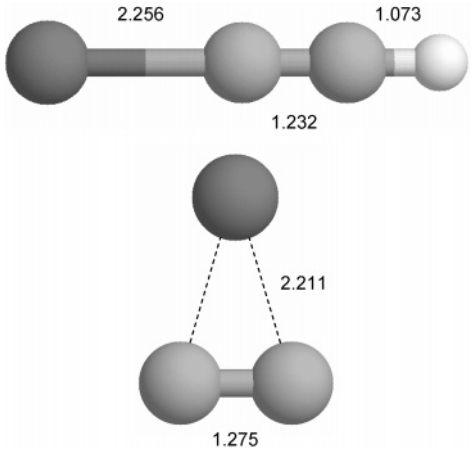


**Figure 2.** B3LYP/aVDZ optimized geometries for $YC_2H$ ($^1\Sigma^+$) and $YC_2$ ($^2A_1$). All distances are reported in Å.

$YC_2H_2$ adduct formation, (ii) C−H insertion, and (iii) Y−H bond cleavage. Details are provided below.

$H_2$ elimination yields yttrium dicarbide, $YC_2$.[24−29] $YC_2$ is a T-shaped molecule with a $^2A_1$ ground electronic state.[26−29] Complete active space self consistent field (CASSCF) calculations of Roszak and Balasubramanian[26] showed that the dicarbide is reasonably well described by single-reference methods, such as those used in this study. We calculate a bond dissociation energy, $D_0$(Y−$C_2$), of 147.7 kcal/mol (with respect to $^2D_{3/2}$ Y and $^1\Sigma_g^+$ $C_2$), in reasonable agreement with experimental estimates of 151 ± 5,[24] 156 ± 5,[25] and 160 ± 5 kcal/mol.[2] NBO analysis calculates the following Lewis representation for $YC_2$.

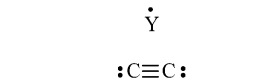

The spin density is largely localized on Y ($\rho_{spin}$ = 0.87) in an orbital of principally (87%) 5s character. The Y−$C_2$ interaction is predominantly electrostatic, resulting from the formal transfer of two electrons from the metal to the ligand. The ionic $M^{2+}/C_2^{2-}$ interaction of metal dicarbides has been proposed previously.[30] Electron density from $C_2^{2-}$ undergoes back donation into vacant or partially filled valence orbitals of Y. Three significant delocalizing interactions are revealed: (i) the in-plane $\pi$ orbital delocalizes into the singly occupied 5s and empty $4d_{z^2}$, (ii) the out-of-plane $\pi$ interacts with the empty $4d_{xz}$, and (iii) the in-phase combination of C lone pairs delocalizes into the 5s orbital. These interactions are largely consistent with the character of the valence molecular orbitals for isovalent $ScC_2$ described by Jackson et al.[28] The interactions collectively back transfer about 0.8 electrons to Y, which has a resulting charge of +1.21.

Two reaction pathways were identified for $H_2$ elimination. The lower energy pathway corresponds to a three step mechanism: (i) $YC_2H_2$ adduct formation, (ii) C−H insertion, and (iii) 1,3-elimination of $H_2$. The highest barrier encountered along this pathway is at 1.0 kcal/mol (relative to reactants) for the 1,3-elimination step. The higher energy pathway is a four-step mechanism: (i) $YC_2H_2$ formation, (ii) C−H insertion, (iii) $\beta$−H transfer, and (iv) reductive elimination of $H_2$. The barriers for the $\beta$−H transfer (11.9 kcal/mol) and reductive elimination (26.4 kcal/mol) steps lie well above the highest barrier encountered in the three step mechanism.

**B. $YC_2H_2$ Adduct Formation.** The Y + $C_2H_2$ reaction begins with the formation of a metallacyclopropene $YC_2H_2$ adduct. Two adducts of $C_{2v}$ symmetry were optimized, a strongly bound $^2A_1$ form (**1a**) at −46.8 kcal/mol and a weakly bound $^2B_2$ form (**1b**) at −25.8 kcal/mol. The energy of $^2A_1$ $YC_2H_2$ agrees well with the −48.6 kcal/mol value determined by Siegbahn[13] using the modified coupled pair functional method. **1a** and **1b** correspond to the ground electronic state of their respective equilibrium geometries. The adducts are separated by a transition state $\mathbf{TS_{add}}$ that lies about 6 kcal/mol above **1b**.

The weakly bound **1b** may form prior to the strongly bound **1a** as Y approaches $C_2H_2$. The **1b** adduct has a nominal $5s^24d^1$ Y configuration that correlates with the ground $^2D$ state of the

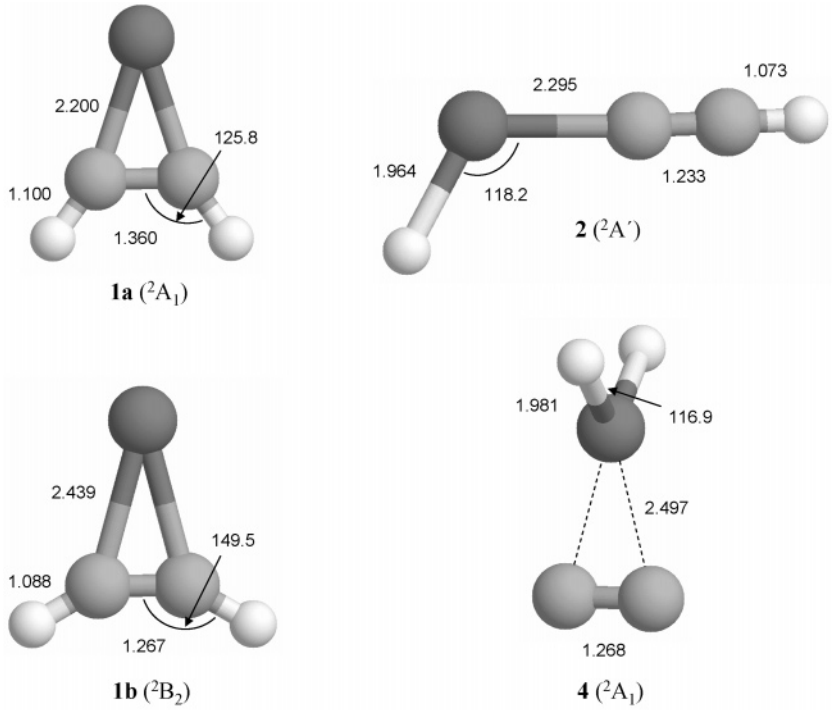


**Figure 3.** B3LYP/aVDZ optimized geometries for the intermediates of the Y + $C_2H_2$ reaction. All distances in Å; angles in degrees.

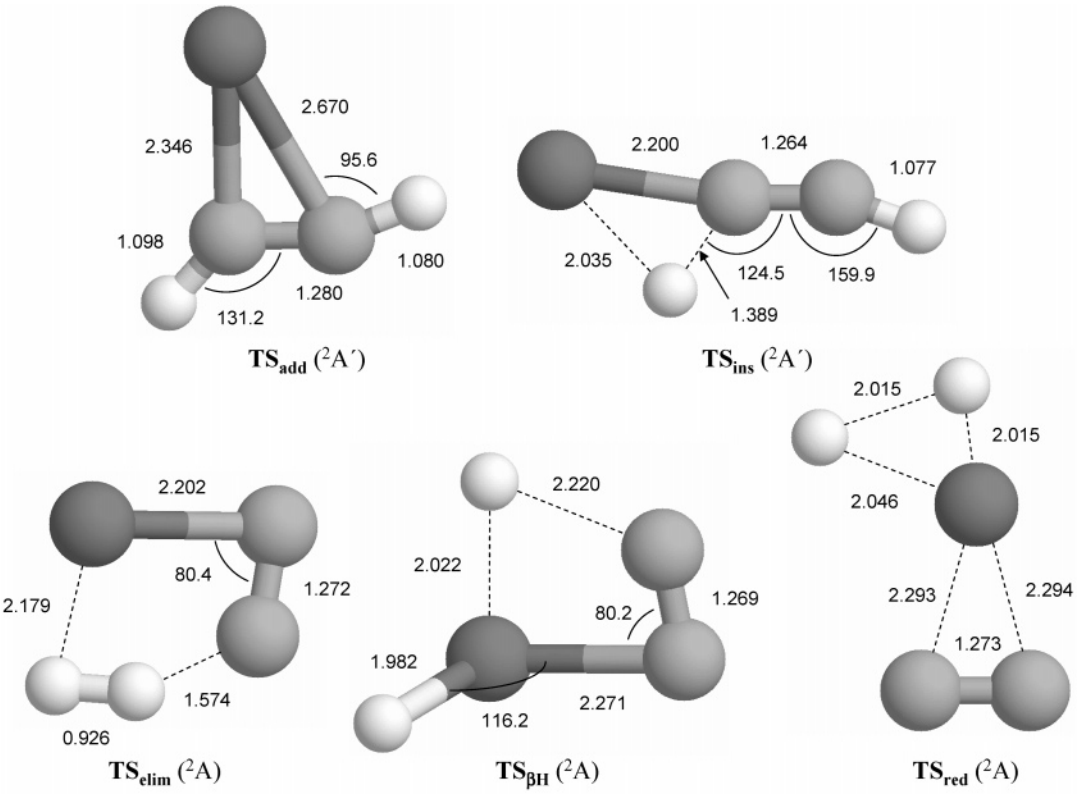


**Figure 4.** B3LYP/aVDZ optimized geometries for the transition states of the Y + $C_2H_2$ reaction. All distances in Å; angle in degrees.

atom. Formation from ground state reactants is likely a barrierless process. Optimization of Y + $C_2H_2$, initially separated by 5 Å, led directly to **1b** along a downhill pathway. In a separate optimization beginning at a 6 Å separation, the metal atom and $C_2H_2$ fragment slowly drifted apart with an energy only marginally greater than that of the separated reactants. Porembski and Weisshaar[3] similarly concluded that the formation of the metallacyclopropane adduct $YC_2H_4$ in Y + $C_2H_4$ reactions proceeds without a barrier.

**1b** exhibits partial metallacyclopropene character consistent with the following Lewis representation:

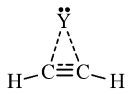


The optimized Y−C bonds are rather long (at 2.439 Å), and the C−C bond length (1.267 Å) is intermediate between that

**TABLE 2: Natural Charges and Spin Densities of the Intermediates, Transition States, and Products of the Y + $C_2H_2$ Reaction**[a]

| | | | natural charges | | | | | natural spin densities | | | | |
|---|---|---|---|---|---|---|---|---|---|---|---|---|
| | structure | state | Y | $C_\alpha$ | $C_\beta$ | H | H′ | Y | $C_\alpha$ | $C_\beta$ | H | H′ |
| **1b** | $YC_2H_2$ | $^2B_2$ | 0.59 | −0.54 | −0.54 | 0.24 | 0.24 | 0.26 | 0.32 | 0.32 | 0.05 | 0.05 |
| **$TS_{add}$** | | $^2A'$ | 0.59 | −0.82 | −0.36 | 0.24 | 0.25 | 0.27 | 0.09 | 0.60 | 0.06 | −0.02 |
| **1a** | $YC_2H_2$ | $^2A_1$ | 1.10 | −0.75 | −0.75 | 0.20 | 0.20 | 0.92 | 0.04 | 0.04 | 0.00 | 0.00 |
| **$TS_{ins}$** | | $^2A'$ | 0.83 | −0.83 | −0.20 | 0.22 | −0.01 | 0.55 | −0.09 | 0.43 | −0.01 | 0.12 |
| **2** | HYC2H | $^2A'$ | 1.33 | −0.73 | −0.24 | 0.23 | −0.58 | 0.96 | 0.02 | 0.00 | 0.00 | 0.02 |
| **$TS_{elim}$** | | $^2A$ | 1.23 | −0.59 | −0.54 | 0.11 | −0.21 | 0.95 | 0.04 | −0.01 | 0.02 | 0.00 |
| **3** | $H_2\cdot\cdot YC_2$ | $^2A_1$ | 1.21 | −0.61 | −0.61 | 0.00 | 0.00 | 0.88 | 0.06 | 0.06 | 0.00 | 0.00 |
| **$TS_\beta H$** | | $^2A$ | 1.71 | −0.58 | −0.24 | −0.34 | −0.56 | 0.01 | 0.11 | 0.66 | 0.22 | 0.00 |
| **4** | $H_2YC_2$ | $^2A_1$ | 1.92 | −0.36 | −0.36 | −0.60 | −0.60 | −0.01 | 0.50 | 0.50 | 0.00 | 0.00 |
| **$TS_{red}$** | | $^2A$ | 1.68 | −0.47 | −0.53 | −0.26 | −0.42 | 0.03 | 0.19 | 0.25 | 0.36 | 0.17 |
| | $YC_2$ | $^2A_1$ | 1.21 | −0.61 | −0.61 | | | 0.87 | 0.06 | 0.06 | | |
| | $YC_2H$ | $^1\Sigma^+$ | 0.75 | −0.75 | −0.22 | 0.23 | | | | | | |
| | $C_2H_2$ | $^1\Sigma_g^+$ | | −0.24 | −0.24 | 0.24 | 0.24 | | | | | |

[a] $C_\alpha$ and H′ refer to the C and H atoms nearer to Y in asymmetric structures.

of standard double (1.335 Å) and triple (1.210 Å) bonds. NBO yields different bonding patterns in the α and $\beta$ spin systems. The α spin system has a C═C double bond and a pair of Y−C single bonds, whereas the $\beta$ spin system has a C≡C triple bond but no Y−C bonds. Average bond orders are, thus, 2.5 for C−C and 0.5 for Y−C, consistent with the intermediate C−C and long Y−C bond lengths. The Y−C bonds of the α system are strongly polarized (85%) toward the C atoms so that Y exhibits a charge of +0.60. The unpaired electron occupies a $b_2$ orbital that is essentially an out-of-phase combination of Y−C bonds. Spin density is thereby delocalized over the Y and C atoms; NPA reports spin densities of 0.26 and 0.32 for the Y and C atoms, respectively. The nonbonding electrons of Y occupy an orbital of principally 5s character.

The more stable **1a** adduct has approximate $5s^14d^2$ character at the metal center that correlates with excited state $^2F$ Y. The optimized Y−C and C−C bond lengths of 2.200 and 1.360 Å, respectively, are consistent with full metallacyclopropene character.

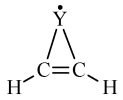

The Y−C bonds are strongly polarized (∼80%) toward the C centers so that Y exhibits a strong positive charge, +1.10. The unpaired electron occupies an $a_1$ orbital that is largely Y 5s, and the spin density is predominantly localized on the Y center ($\rho_{spin} = 0.92$).

Adduct **1a** likely forms from electronic rearrangement of **1b**. **1b** is converted to **1a** via a $C_s$ pathway through a $^2A'$ transition state **$TS_{add}$**. We were unable to fully converge **$TS_{add}$** at the B3LYP/aVDZ level. UHF/3-21G calculations of the transition state converged a $C_s$ structure, but further refinement with B3LYP/aVDZ failed to locate a saddle point. Instead, the B3LYP optimization oscillated (by ±0.1 kcal/mol) about the structure shown in Figure 4. The forces and displacements reported by Gaussian 98 were generally an order of magnitude larger than threshold values. The geometrical features of **$TS_{add}$** appear reasonable, with Y−C and C−C bond lengths (2.346 and 1.280 Å, respectively) intermediate between those of **1a** and **1b**. We suspect that the true B3LYP/aVDZ transition state lies near **$TS_{add}$** and is of similar energy, −19.3 kcal/mol relative to reactants, or about 6 kcal/mol above **1b**.

By breaking the $C_{2v}$ symmetry of **1b**, the $C_s$ pathway through **$TS_{add}$** enables the redistribution of $\beta$ electrons required to increase the metallacyclopropene character of the adduct from partial ($^2B_2$) to full ($^2A_1$). Two $\beta$ electrons of **1b**, each occupying $a_1$-type orbitals, are involved in the redistribution. These include the nonbonding 5s electron on Y and the in-plane $\pi$ electron of $C_2H_2$. Redistribution allows these "chemically active" electrons to eventually occupy the in-phase ($a_1$) and out-of-phase ($b_2$) combinations of Y−C bonds in **1a**. Analysis of the NLMOs for **$TS_{add}$** reveals the following electron redistribution.

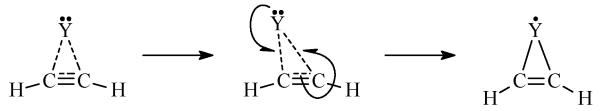

Conventional fishhook arrows are used here to indicate the movements of single electrons. As Y moves off the $C_2$ symmetry axis, the 5s $\beta$ electron increasingly delocalizes into the in-plane $\pi^*$ orbital of $C_2H_2$, eventually forming a Y−C bond and cleaving the $\pi$ bond. Simultaneously, the $\beta$ electron of the in-plane $\pi$ orbital undergoes back donation into a Y 4d hybrid, forming a second Y−C bond. No redistribution of α electrons is seen in the analysis.

**C. C−H Insertion.** Y inserts into a C−H bond of $C_2H_2$, forming the $HYC_2H$ intermediate **2**. This insertion step starts from the $^2A_1$ form (**1a**) of the $YC_2H_2$ adduct and proceeds along a $C_s$ pathway through transition state **$TS_{ins}$**. The barrier is 44.1 kcal/mol relative to **1a**. Insertion is somewhat endothermic (by 4.7 kcal/mol) with the intermediate **2** lying 42.1 kcal/mol below reactants. Siegbahn[13] reports MCPF results that suggest a 53.9 kcal/mol barrier and endothermicity of 7.2 kcal/mol. NBO analysis calculates the following Lewis structure for **2**.

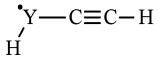

Y interacts with the acetylide and hydride ligands through Y−C and Y−H bonds that are strongly polarized toward the C and H atoms (by ∼88% and ∼80%, respectively). The unpaired electron is essentially localized on Y ($\rho_{spin} = 0.96$) in a hybrid of largely (70%) 5s character.

IRC calculations identified a $C_s$ pathway that interconverts the $^2A_1$ form of $YC_2H_2$ and the $^2A'$ intermediate **2**, proceeding via the $^2A'$ transition state **$TS_{ins}$**. The reaction along this pathway proceeds as follows.

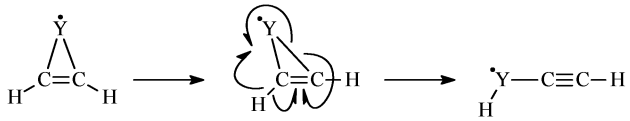

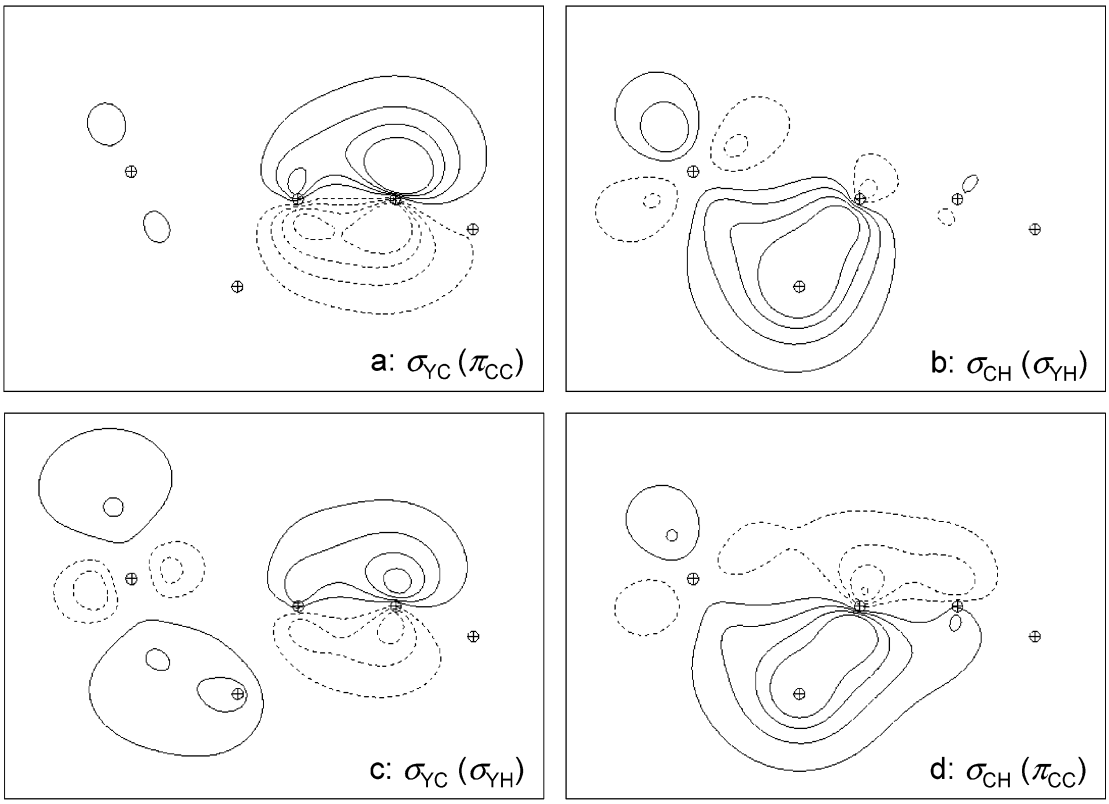


**Figure 5.** Contour diagrams of the chemically active NLMOs of $\mathbf{TS_{ins}}$. Diagrams a and b are of α spin NLMOs; diagrams c and d are $\beta$ spin. The orbital character in the $YC_2H_2$-like analysis of $\mathbf{TS_{ins}}$ is noted. The corresponding character for the $HYC_2H$-like analysis is given in parentheses. Markers (⊕) indicate the locations of the nuclei in the same orientation as $\mathbf{TS_{ins}}$ in Figure 2.

In the orientation shown here, the Y center moves counterclockwise about $C_\alpha$ and inserts into the $C_\alpha-H$ bond. Four electrons (those of the $Y-C_\beta$ and $C_\alpha-H$ bonds) undergo simultaneous redistribution during the reaction. The bonds cleave homolytically, the α and $\beta$ density redistributing in opposing directions. The two arrows directed in a clockwise fashion represent α electrons; the two directed counterclockwise represent $\beta$. Figure 5 shows contour diagrams of the NLMOs in $\mathbf{TS_{ins}}$ for the four electrons.

The α system exhibits the rearrangement of two electrons. As Y moves away from $C_\beta$, the $Y-C_\beta$ bond polarizes toward $C_\beta$ and increasingly delocalizes into the $C_\alpha-H$ $\sigma^*$ antibond. The strengthening $\sigma_{YC} \rightarrow \sigma_{CH}^*$ interaction cleaves the $Y-C_\beta$ bond by depleting its orbital of electron density, promotes the fission of the $C_\alpha-H$ bond by populating its antibond, and results in the eventual formation of an in-plane $\pi$-bond through the overlap of the C hybrids of the $Y-C_\beta$ and $C_\alpha-H$ bonds. Figure 5a shows the corresponding NLMO. Though this orbital correlates with the $Y-C_\beta$ bond of **1a**, only marginal Y character remains in the transition state. The orbital is largely localized on $C_\beta$ and the in-plane $\pi$-type interaction with $C_\alpha$ is apparent. Meanwhile, the α electron of the $C_\alpha-H$ bond increasingly delocalizes into a vacant Y 4d orbital as Y moves toward H. The C−H bond cleaves as electron density is removed from $\sigma_{CH}$ (and density accumulates in $\sigma_{CH}^*$ from $\sigma_{YC}$) and a Y−H bond forms. Figure 5b shows the NLMO for this electron. Significant bonding character remains between H and $C_\alpha$ but the strengthening covalent interaction with the Y 4d is clear.

The $Y-C_\beta$ and $C_\alpha-H$ electrons of the $\beta$ system also undergo redistribution. Their respective NLMOs are shown in Figures 5c and 5d. As Y moves away from $C_\beta$, the $Y-C_\beta$ bond polarizes toward Y and eventually delocalizes into the $C_\alpha-H$ antibond. The $\sigma_{YC} \rightarrow \sigma_{CH}^*$ interaction cleaves the $Y-C_\beta$ bond by depleting it of electron density, weakens the $C_\alpha-H$ bond by populating its antibond, and eventually leads to the formation of a Y−H bond. Figure 5c shows the corresponding NLMO. While the orbital still retains significant $C_\beta$ character, the onset of Y−H covalent interaction involving a Y sd hybrid and a H 1s orbital is apparent. As the $Y-C_\beta$ electron is redistributed to form the Y−H bond, the $C_\alpha-H$ electron moves to form the in-plane $\pi$-bond. As shown in Figure 5d, the $C_\alpha-H$ electron delocalizes into a p-type orbital on $C_\beta$, the remnant of the $Y-C_\beta$ antibond.

Insertion intermediate **2** can undergo Y−H dissociation, yielding the H atom elimination products $YC_2H + H$. Attempts to optimize a $YC_2H + H$ product complex failed. Geometries corresponding to this complex consistently collapsed along a downhill pathway to the covalently bonded $HYC_2H$ structure **2**. Thus, there appears to be no barrier to Y−H bond fission in excess of the reaction endothermicity. Our best estimate of the $H-YC_2H$ bond dissociation energy ($D_0$) is 57.1 kcal/mol.

**D. 1,3-Elimination of $H_2$.** Insertion intermediate **2** can undergo 1,3-elimination, yielding the $YC_2 + H_2$ product complex **3**. This $C_{2v}$ complex results from the weak association of $YC_2$ and $H_2$ molecules. The $YC_2$ geometry is essentially identical to that shown in Figure 2; the $H_2$ molecule is ca. 6.8 Å from the Y atom in a plane perpendicular to the $YC_2$ plane. Due to the zero point energy correction, the product complex lies 0.1 kcal/mol above the separated products, suggesting that the complex dissociates without a barrier.

The 1,3-elimination step proceeds via a $C_1$ pathway through the transition state $\mathbf{TS_{elim}}$. The reaction is strongly endothermic (by 35.1 kcal/mol) and proceeds over a barrier of 43.1 kcal/mol. We note that $\mathbf{TS_{elim}}$ lies only 1.0 kcal/mol above the separated reactants. The barrier associated with this transition state is the highest that is encountered along the three step $H_2$

elimination pathway. The crossed molecular beams study of Davis et al.[2] yielded an upper limit of 6 kcal/mol for the $H_2$ elimination barrier, slightly higher than the 1.0 kcal/mol value we calculate. $\mathbf{TS_{elim}}$ is a cyclic, multicenter transition state similar to those previously identified by Porembski and Weisshaar[3] for $H_2$ elimination in $Y + C_2H_4$ reactions and by Bayse[31] for elimination in $Y + H_2CO$.

The 1,3-elimination of $H_2$ proceeds as follows.

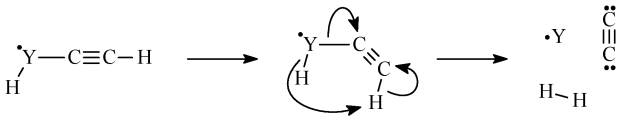

In the representation shown, the H atom of the acetylide group shifts downward and to the left, approaching the Y-bonded H atom. Full-headed arrows are drawn to indicate the redistribution of electron pairs. As the two H atoms approach each other, the pair of electrons of the Y−H bond (which is strongly polarized toward H) begin to delocalize into the $C_\beta$−H antibond of the acetylide group. This transfer of electron density weakens the Y−H bond (eventually cleaving it), weakens the $C_\beta$−H bond (by populating the antibond), and strengthens the covalent interaction of the two H atoms (through the overlap of 1s orbitals), leading to $H_2$ formation and elimination. Meanwhile, the electrons of the Y−$C_\alpha$ and $C_\beta$−H bonds polarize toward their respective C centers, cleaving the bonds and giving rise to the two lone pairs of the $C_2$ ligand (of the $YC_2$ complex). Unlike the homolytic cleavage of bonds observed for the C−H insertion reaction, the 1,3-elimination step involves heterolytic bond cleavage in which electron pairs move together, undergoing redistribution in the same direction. The unpaired electron does not appear to participate significantly in 1,3-elimination; it remains localized on Y throughout the reaction step in an orbital of principally 5s character.

**E. $\beta$−H Transfer.** The HYCCH intermediate **2** can alternatively undergo $\beta$−H transfer instead of 1,3-elimination. The step proceeds along a $C_1$ pathway through $\mathbf{TS_{\beta H}}$. The H atom on $C_\beta$ transfers to Y yielding the dihydrido intermediate $H_2YC_2$, **4**. $\mathbf{TS_{\beta H}}$ lies 11.9 kcal/mol above reactants, or nearly 11 kcal/mol above $\mathbf{TS_{elim}}$ for the 1,3-elimination step. 1,3-elimination is clearly favored over $\beta$−H transfer. The $C_{2v}$ dihydrido intermediate **4** lies 3.5 kcal/mol above the reactants. No lower symmetry intermediate could be identified. CAS calculations of **4** (active space: $6a_1^2\ 3b_2^2\ 3b_1^2\ 7a_1^1\ 4b_2^0\ 8a_1^0$) yield a leading CI coefficient of 0.974, suggesting that single-reference methods provide an adequate description.

NBO analysis of **4** suggests the following Lewis representation that reflects the transfer of one electron from the $YH_2$

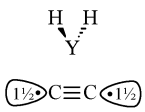

fragment to $C_2$. The C nonbonding hybrids have formal occupancies of 1.5 electrons each. Two α electrons occupy the in-phase and out-of-phase combinations of these orbitals, whereas the $\beta$ electron occupies only the out-of-phase combination. Spin density is equally distributed between the C atoms ($\rho_{spin}(C) = 0.50$). The charge on Y is 1.92, largely the result of electron transfer to $C_2$ and the strong polarization (by 80%) of the Y−H bonds toward H.

Analysis of $\mathbf{TS_{\beta H}}$ reveals the following redistribution of electron density. The H and $C_\beta$ atoms of the acetylide group shift toward Y as the H atom begins to transfer to the metal.

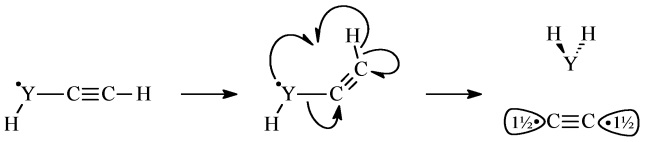

Arrows directed in a clockwise fashion correspond to the movements of α spin electrons; arrows directed counterclockwise are $\beta$. As the H atom approaches the metal center, the unpaired α electron on Y begins to delocalize into the C−H antibond. The $\beta$ electron of the C−H bond simultaneously delocalizes into a vacant 4d orbital on Y. These interactions give rise to the Y−H bond while cleaving the C−H bond. The α electron of the C−H bond becomes a nonbonding electron on $C_\beta$. The Y−C bond cleaves as its electrons move into a nonbonding sp hybrid on $C_\alpha$.

**F. Reductive Elimination of $H_2$.** The dihydrido intermediate **4** can eliminate $H_2$ to give the $YC_2 + H_2$ products. A transition state, $\mathbf{TS_{red}}$, was identified for this reaction step, lying 22.9 kcal/mol above **4**, or 26.4 kcal/mol above reactants. $\mathbf{TS_{red}}$ corresponds to the highest barrier encountered in the four step elimination mechanism. IRC calculations show that $\mathbf{TS_{red}}$ lies along a $C_1$ pathway connecting **4** to the $C_{2v}$ product complex **3**. NBO analysis suggests the following redistribution of electrons (the α electron density shifting in a clockwise fashion, the $\beta$ density counterclockwise).

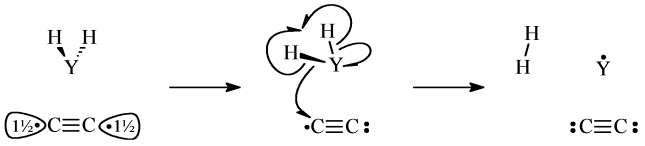

The Y−H bonds cleave homolytically, forming the $H_2$ molecule and transferring a $\beta$ electron into an in-phase combination of nonbonding hybrids on $C_2$.

An alternative elimination mechanism can be considered in which $H_2$ is lost from the dihydrido complex along a $C_{2v}$ symmetry pathway. Though the ground states of the dihydrido complex **4** and product complex **3** are both of $^2A_1$ symmetry, their respective electron configurations, $(3b_2)^2(6a_1)^2(2b_1)^2(7a_1)^2(8a_1)^1$ and $(3b_2)^2(6a_1)^2(2b_1)^2(3b_1)^2(7a_1)^1$, differ by the double occupancy of an $a_1$ and $b_1$ orbital. Treating the elimination of $H_2$ along the symmetric pathway requires a multiconfiguration approach that includes at least these two configurations. Bayse[31] considered the symmetric elimination of $H_2$ in $Y + H_2CO$ reactions, using complete active space selfconsistent field (CASSCF) calculations. Our attempts to use CASSCF to identify a symmetric transition state of $H_2$ elimination in $Y + C_2H_2$ were unsuccessful.

## IV. Conclusions

Pathways for H atom and $H_2$ elimination in the reaction of ground state Y atom with $C_2H_2$ have been calculated. The lower energy $H_2$ elimination pathway proceeds in three steps: (i) $YC_2H_2$ adduct formation, (ii) C−H insertion, and (iii) 1,3-elimination of $H_2$. The higher energy H atom elimination reaction follows a similar three step mechanism, but undergoes, in its last step, Y−H bond fission from the C−H insertion intermediate. $H_2$ elimination is exothermic (at 0 K) by 7.1 kcal/mol, and the highest barrier encountered along this pathway is at 1.0 kcal/mol in the 1,3-elimination step. H atom elimination, a competing pathway, is endothermic by 15.0 kcal/mol; no barrier is encountered in excess of this endothermicity.

Our calculated reaction profile (Figure 1) can be compared with the results of the crossed molecular beam work of Davis et al.[2] Several favorable points of comparison can be noted. First, $YC_2 + H_2$ products were observed in the experiments at all collision energies from 6 to 25 kcal/mol; 6 kcal/mol was thus assigned as an upper limit for the $H_2$ elimination barrier. The highest calculated barrier for this pathway is 1.0 kcal/mol for the 1,3-elimination step, consistent with the 6 kcal/mol upper bound. Second, kinetic energy distributions suggest the existence of a significant potential energy barrier in the exit channel for $H_2$ elimination. Indeed, we find that the barrier for the 1,3-elimination step lies ca. 8 kcal/mol above the $YC_2 + H_2$ products. Third, $YC_2H + H$ products were only observed at high collision energies, resulting from the dissociation of the Y−H bond in the $HYC_2H$ insertion intermediate. The calculated reaction pathway supports this observation.

Our reaction profile differs, however, in some important respects from that proposed previously. Most significantly, whereas we calculate the $YC_2 + H_2$ and $YC_2H + H$ product asymptotes at −7.1 and 15.0 kcal/mol, respectively, Stauffer et al.[2] report energies of $-18.5 \pm 4.3$ and $21.5 \pm 2.0$ kcal/mol. The origin of these large discrepancies is unclear. Also, the mechanism we calculate for $H_2$ elimination differs from that proposed. A four step mechanism was suggested in which the last two steps are (proceeding from the insertion intermediate) $\beta$-H transfer and reductive elimination. Calculations for these steps yielded barriers of 11.9 and 26.4 kcal/mol, respectively, well above the 6 kcal/mol upper limit. $H_2$ elimination more likely proceeds via the three step mechanism for which the last (and rate limiting) step is 1,3-elimination. Similar mechanisms have been proposed for $H_2$ elimination in $Y + C_2H_4$[3] and $Y + CH_2O$.[31]

Finally, the Y atom is intimately involved in most of the reaction steps for H atom and $H_2$ elimination. The open shell character of the metal atom and vacant 4d orbitals tend to promote homolytic bond cleavage and formation along the reaction pathways. The exception is the 1,3-elimination step for which bonds cleave heterolytically.

**Acknowledgment.** The author gratefully acknowledges Kirk Peterson (Washington State University) for advice regarding MOLPRO and basis set extrapolations. Prof. Peterson kindly provided his cc-pV*X*Z-PP basis sets and correlating functions for Y prior to their publication. Partial support for this work was provided by the National Science Foundation's Division of Undergraduate Education through Grant DUE #98-51497.

## References and Notes

(1) Carroll, J. J.; Haug, K. L.; Weisshaar, J. C. *J. Phys. Chem.* **1995**, *99*, 13955.
(2) Stauffer, H. U.; Hinrichs, R. Z.; Willis, P. A.; Davis, H. F. *J. Chem. Phys.* **1999**, *111*, 4101.
(3) Porembski, M.; Weisshaar, J. C. *J. Phys. Chem. A* **2001**, *105*, 6655.
(4) Stauffer, H. U.; Hinrichs, R. Z.; Schroden, J. J.; Davis, H. F. *J. Phys. Chem. A* **2000**, *104*, 1107.
(5) Hinrichs, R. Z.; Schroden, J. J.; Davis, H. F. *J. Am. Chem. Soc.* **2003**, *125*, 860.
(6) Wen, Y.; Porembski, M.; Ferrett, T. A.; Weisshaar, J. C. *J. Phys. Chem. A* **1998**, *102*, 8362.
(7) Willis, P. A.; Stauffer, H. U.; Hinrichs, R. Z.; Davis, H. F. *J. Phys. Chem. A* **1999**, *103*, 3706.
(8) (a) Porembski, M.; Weisshaar, J. C. *J. Phys. Chem. A* **2000**, *104*, 1524. (b) Porembski, M.; Weisshaar, J. C. *J. Phys. Chem. A* **2001**, *105*, 4851.
(9) (a) Willis, P. A.; Stauffer, H. U.; Hinrichs, R. Z.; Davis, H. F. *J. Chem. Phys.* **1998**, *108*, 2665. (b) Hinrichs, R. Z.; Willis, P. A.; Stauffer, H. U.; Schroden, J. J.; Davis, H. F. *J. Chem. Phys.* **2000**, *112*, 4634.
(10) Stauffer, H. U.; Hinrichs, R. Z.; Schroden, J. J.; Davis, H. F. *J. Chem. Phys.* **1999**, *111*, 10758.
(11) Schroden, J. J.; Teo, M.; Davis, H. F. *J. Chem. Phys.* **2002**, *117*, 9258.
(12) Schroden, J. J.; Teo, M.; Davis, H. F. *J. Phys. Chem. A* **2002**, *106*, 11695.
(13) Siegbahn, P. E. M. *Theor. Chim. Acta* **1994**, *87*, 277.
(14) Siegbahn, P. E. M. *J. Phys. Chem.* **1995**, *99*, 12723.
(15) Glendening, E. D.; Strange, M. L. *J. Phys. Chem. A* **2002**, *106*, 7338.
(16) (a) Becke, A. D. *J. Chem. Phys.* **1993**, *98*, 5648. (b) Lee, C.; Yang, W.; Parr, R. G. *Phys. Rev. B* **1988**, *37*, 785. (c) Vosko, S. H.; Wilk, L.; Nusair, M. *Can. J. Phys.* **1980**, *58*, 1200. (d) Stephens, P. J.; Devlin, F. J.; Chabalowski, C. F.; Frisch, M. J. *J. Phys. Chem.* **1994**, *98*, 11623.
(17) (a) Dunning, T. H., Jr. *J. Chem. Phys.* **1989**, *90*, 1007. (b) Kendall, R. A.; Dunning, T. H., Jr.; Harrison, R. J. *J. Chem. Phys.* **1992**, *96*, 6796.
(18) Andrae, D.; Haeussermann, U.; Dolg, M.; Stoll, H.; Preuss, H. *Theor. Chim. Acta* **1990**, *77*, 123.
(19) Peterson, K. A., private communication.
(20) Frisch, M. J.; Trucks, G. W.; Schlegel, H. B.; Scuseria, G. E.; Robb, M. A.; Cheeseman, J. R.; Zakrzewski, V. G.; Montgomery, J. A., Jr.; Stratmann, R. E.; Burant, J. C.; Dapprich, S.; Millam, J. M.; Daniels, A. D.; Kudin, K. N.; Strain, M. C.; Farkas, O.; Tomasi, J.; Barone, V.; Cossi, M.; Cammi, R.; Mennucci, B.; Pomelli, C.; Adamo, C.; Clifford, S.; Ochterski, J.; Petersson, G. A.; Ayala, P. Y.; Cui, Q.; Morokuma, K.; Malick, D. K.; Rabuck, A. D.; Raghavachari, K.; Foresman, J. B.; Cioslowski, J.; Ortiz, J. V.; Baboul, A. G.; Stefanov, B. B.; Liu, G.; Liashenko, A.; Piskorz, P.; Komaromi, I.; Gomperts, R.; Martin, R. L.; Fox, D. J.; Keith, T.; Al-Laham, M. A.; Peng, C. Y.; Nanayakkara, A.; Gonzalez, C.; Challacombe, M.; Gill, P. M. W.; Johnson, B.; Chen, W.; Wong, M. W.; Andres, J. L.; Gonzalez, C.; Head-Gordon, M.; Replogle, E. S.; Pople, J. A. *Gaussian 98*, Rev A.7; Gaussian, Inc., Pittsburgh, PA, 1998.
(21) (a) Peterson, K. A.; Woon, D. E.; Dunning, T. H., Jr. *J. Chem. Phys.* **1994**, *100*, 7410. (b) Woon, D. E.; Dunning, T. H., Jr. *J. Chem. Phys.* **1994**, *101*, 8877.
(22) (a) MOLPRO is a package of ab initio programs written by H.-J. Werner and P. J. Knowles with contributions from J. Almlof, R. D. Amos, A. Berning, D. L. Cooper, M. J. O. Deegan, A. J. Dobblyn, F. Eckert, S. T. Elbert, C. Hampel, R. Lindh, A. W. Lloyd, W. Meyer, A. Nicklass, K. Peterson, R. Pitzer, A. J. Stone, P. R. Taylor, M. E. Mura, P. Pulay, M. Schutz, H. Stoll, and T. Thorsteinsson. (b) Hampel, C.; Peterson, K.; Werner, H.-J. *Chem. Phys. Lett.* **1992**, *190*, 1. (c) Knowles, P. J.; Hampel, C.; Werner, H.-J. *J. Chem. Phys.* **1993**, *99*, 5219.
(23) (a) Glendening, E. D.; Badenhoop, J. K.; Reed, A. E.; Carpenter, J. E.; Bohmann, J. A.; Morales, C. M.; Weinhold, F. *NBO 5.0*; Theoretical Chemistry Institute, University of Wisconsin, Madison, WI, 2001. (b) Reed, A. E.; Curtiss, L. A.; Weinhold, F. *Chem. Rev.* **1988**, *88*, 899. (c) Reed, A. E.; Weinhold, F. *J. Chem. Phys.* **1985**, *83*, 1736. (d) Reed, A. E.; Weinhold, F. *J. Chem. Phys.* **1983**, *78*, 4066.
(24) Gupta, S. K.; Gingerich, K. A. *J. Chem. Phys.* **1981**, *74*, 3584.
(25) De Maria, G.; Guido, M.; Malaspina, L.; Pesce, B. *J. Chem. Phys.* **1965**, *43*, 4449.
(26) Roszak, S.; Balasubramanian, K. *Chem. Phys. Lett.* **1995**, *246*, 20.
(27) Steimle, T. C.; Marr, A. J.; Xin J.; Merer, A. J.; Athanassenas, K.; Gillett, D. *J. Chem. Phys.* **1997**, *106*, 2060.
(28) Jackson, P.; Gadd, G. E.; Mackey, D. W.; van der Wall, H.; Willett, G. D. *J. Phys. Chem. A* **1998**, *102*, 8941.
(29) Bousquet, R. R.; Steimle, T. C. *J. Chem. Phys.* **2001**, *114*, 1306.
(30) Chupka, W. A.; Berkowitz, J.; Giese, C. F.; Inghram, M. G. *J. Phys. Chem.* **1958**, *62*, 611.
(31) Bayse, C. A. *J. Phys. Chem. A* **2002**, *106*, 4226.